Journal of Magnetic Resonance 209 (2011) 337–340

Contents lists available at ScienceDirect

Journal of Magnetic Resonance

journal homepage: www.elsevier.com/locate/jmr

Communication

Optimization of magnetic field sweep and field modulation amplitude for continuous-wave EPR oximetry

J. Palmer [a], L.C. Potter [a], R. Ahmad [b,*]

[a] Department of Electrical and Computer Engineering, The Ohio State University, Columbus, OH 43210, USA
[b] Center of Biomedical EPR Spectroscopy and Imaging, Davis Heart and Lung Research Institute, Department of Internal Medicine, The Ohio State University, Columbus, OH 43210, USA

ARTICLE INFO

Article history:
Received 6 October 2010
Revised 22 November 2010
Available online 26 January 2011

Keywords:
EPR
Spectroscopy
Oximetry
Overmodulation
Cramér-Rao lower bound

ABSTRACT

For continuous-wave electron paramagnetic resonance spectroscopy, what settings of magnetic field sweep width and field modulation amplitude yield the best accuracy in estimated linewidth? Statistical bounds on estimation error presented in this work provide practical guidance: set the sweep width and modulation amplitude to 8 and 4 times the half-width half-maximum linewidth, Γ, respectively. For unknown linewidths in the range $[\Gamma_{\min}, \Gamma_{\max}]$ the worst-case estimation error is minimized by using settings designed for $\Gamma_{\max}$. The analysis assumes a Lorentzian lineshape and a constant modulation amplitude across the extent of the irradiated paramagnetic probe. The analytical guidelines are validated using L-band spectroscopy with a particulate LiNc-BuO probe.

© 2011 Elsevier Inc. All rights reserved.

1. Introduction

Electron paramagnetic resonance (EPR) is a spectroscopic method capable of detecting free radicals. Over the past several decades, EPR has found numerous applications in biology, chemistry, physics, and medicine [1]. For biological applications, such as *in vivo* oximetry [2–4], there exists a pressing need to accelerate data acquisition for EPR spectroscopy and imaging [5].

For continuous-wave (CW) EPR, it is a universal practice to apply magnetic field modulation and phase sensitive detection [6]. To improve signal-to-noise ratio (SNR), the modulation amplitude, B_m, is generally increased to a level where it approaches or exceeds the intrinsic half-width half-maximum (HWHM) linewidth, Γ, of the EPR probe. Such B_m values, however, introduce lineshape distortion. Although modulation-induced distortion itself is well characterized [7–9], a theoretical basis for selecting an optimal value of B_m has been missing from the EPR literature.

EPR oximetry [4] entails quantifying oxygen levels by measuring the oxygen-induced linewidth broadening of oxygen-sensitive EPR probes. For EPR oximetry, an allowable scan time is limited by application. Here, we ask the question, "How are magnetic field sweep width, Δ_B, and field modulation amplitude, B_m, set for best sensitivity in inferring linewidth?" We use the Cramér-Rao lower bound (CRLB) to predict the standard deviation of linewidth estimation error as a function of Γ, Δ_B, B_m, signal intensity d, and noise standard deviation σ. The CRLB sets a lower bound on the error standard deviation for any unbiased estimator. The experiment parameters, Δ_B and B_m, are chosen to minimize this bound and hence provide the most accurate linewidth estimation for a given scan time. Our analysis is valid for a Lorentzian lineshape and a spatially-invariant field modulation amplitude across all the irradiated spins.

2. Theory and methodology

2.1. Assumptions and models

The following assumptions are employed in our analysis: (i) the value of Γ is unknown but resides in a known range, $\Gamma_{\min}$ to $\Gamma_{\max}$; (ii) the center field of the lineshape is known; (iii) the signal intensity d is unknown and proportional to spin density; (iv) the unknown value of B_m is spatially uniform across all irradiated spins; (v) the field sweep rate is sufficiently slow to not fall into the rapid-scan regime [10]; (vi) and the lineshape is a modulation-distorted first-harmonic Lorentzian.

When the ratio of field modulation frequency and gyromagnetic ratio is negligible compared to Γ, the resulting modulation-distorted lineshape can be expressed using a simplified version of the model reported by Robinson et al. [8].

$$f(B; d, \Gamma, B_m) = \mathrm{Im}\left(\frac{dB_m}{\alpha}\right) \quad (1)$$

* Corresponding author. Address: 420 W 12th Ave., Suite 126A, Columbus, OH 43210, USA. Fax: +1 614 292 8454.
E-mail address: rizwan.ahmad@osumc.edu (R. Ahmad).

1090-7807/$ - see front matter © 2011 Elsevier Inc. All rights reserved.
doi:10.1016/j.jmr.2011.01.013

where

$$\alpha = \frac{a^2}{2}\left(1+\sqrt{1-\left(\frac{B_m}{2a}\right)^2}\right) - \frac{B_m^2}{8}, \quad \text{with } a = B + j\Gamma.$$

Here, f is the modulation-distorted first-harmonic Lorentzian lineshape, B is the applied magnetic field, j denotes the imaginary unit, and Im(·) represents the imaginary part. Fig. 1 shows simulated f for various levels of modulation.

A scan is composed of M successive data points, called measurements, taken at regular intervals across the field sweep. The measured data are given by:

$$Y_i = f(B_i; d, \Gamma, B_m) + N_i \equiv f_i + N_i, \tag{2}$$

where

$$B_i = \frac{i\Delta_B}{M-1} - \frac{\Delta_B}{2}, \tag{3}$$

$i \in \{0,\ldots,M-1\}$, and N_i is additive white Gaussian noise [11]. The noise standard deviation, σ, is proportional to $\sqrt{T}$, with T being the scan time. When comparing two measurements with different B_m and Δ_B, the values of both M and T are fixed.

2.2. CRLB analysis

The CRLB is computed from the inverse of the Fisher information matrix, I [12]. Let $p(\vec{Y}|\vec{\theta})$ be the probability density function of the data $\vec{Y} = [Y_0, \cdots, Y_{M-1}]$ conditioned on parameters $\vec{\theta}$, with $\vec{\theta} = [d, \Gamma, B_m]$, and let $E_{\vec{Y}}[\cdot]$ denote the expectation over $\vec{Y}$. Then the elements of the Fisher information matrix according to Eq. (2) are as follows:

$$\begin{aligned}(I(\vec{\theta}))_{k,l} &= -E_{\vec{Y}}\left[\frac{\partial^2}{\partial\theta_k\partial\theta_l}\log\left(p(\vec{Y}|\vec{\theta})\right)\right] \\ &= \frac{1}{2\sigma^2}E_{\vec{Y}}\left[\sum_i \frac{\partial}{\partial\theta_k}\frac{\partial}{\partial\theta_l}(Y_i - f_i)^2\right] \\ &= \frac{1}{\sigma^2}\sum_i\left(\frac{\partial}{\partial\theta_k}f_i\right)\left(\frac{\partial}{\partial\theta_l}f_i\right).\end{aligned} \tag{4}$$

Eq. (4) is valid for any signal model f and can also be extended, if required, to include other measurement parameters such as modulation frequency, unknown center field, and parametric baseline distortion. The CRLB on the standard deviation of the estimated linewidth $\widehat{\Gamma}$ is then the square-root of the second element along the diagonal of the inverse of I:

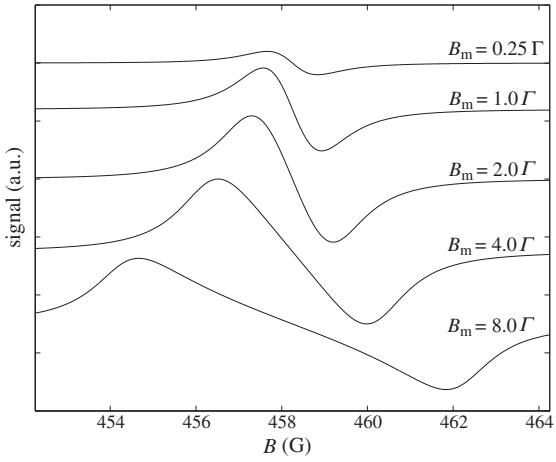

Fig. 1. Simulated first-harmonic Lorentzian lineshape (Eq. (1)) in the presence of various levels of field modulation. Here, $\Gamma = 1$, center field is 458.25 G, and $\Delta_B = 12$ G. The peak signal intensity is maximum at $B_m = 4.0\Gamma$.

$$\mathrm{CRLB}_{\widehat{\Gamma}}(d, \Gamma, B_m, \Delta_B, \sigma) = \sqrt{(I^{-1})_{2,2}}. \tag{5}$$

For brevity, the left side of Eq. (5) will be referred to as $\mathrm{CRLB}_{\widehat{\Gamma}}$. A combination of B_m and Δ_B that yields minimum $\mathrm{CRLB}_{\widehat{\Gamma}}$ is selected as optimal. Noisy measurements, $\vec{Y}$, are then collected using these optimal values. The unknown linewidth is estimated via a least-squares curve fit of $\vec{Y}$ to the model in Eq. (1). The precise value of modulation amplitude, which is generally not known accurately, is jointly estimated along with the other unknown parameters, yielding,

$$\widehat{\vec{\theta}} = \arg\min_{\vec{\theta}} \sum_{i=0}^{M-1}(f_i - Y_i)^2, \tag{6}$$

where, $\widehat{\vec{\theta}} = [\hat{d}, \widehat{\Gamma}, \widehat{B}_m]$, with $\hat{d}, \widehat{\Gamma}$, and $\widehat{B}_m$ being the estimated values of signal intensity, HWHM linewidth, and modulation amplitude, respectively.

2.3. Experimental setup

For verification, findings from the CRLB analysis were compared to experimentally observed linewidth estimation errors. A small single crystal of LiNc-BuO [13], under anoxic conditions, was used to collect data on a CW L-band (1.28 GHz) system using a volume loop-gap resonator. The anoxic linewidth of the probe (0.315 G) was known in advance. Other system parameters were as follows: 2 mW radio frequency power; 0.16 G/$\sqrt{\mathrm{W}}$ resonator efficiency [14]; 100 kHz field modulation frequency; 3.9 s scan time; and 1024 samples per scan.

3. Results

3.1. Theoretical and simulated

The value of $\mathrm{CRLB}_{\widehat{\Gamma}}$, computed from Eq. (5), varies as a function of d, Γ, B_m, Δ_B, and σ. However, the location of the minimum does not vary with B_m/Γ and Δ_B/Γ, at least not over the range of Γ experienced in EPR oximetry. Fig. 2 shows how $\mathrm{CRLB}_{\widehat{\Gamma}}$ varies with B_m/Γ and Δ_B/Γ. The minimum $\mathrm{CRLB}_{\widehat{\Gamma}}$ occurs at approximately

$$\begin{aligned}&\Delta_B = 8\Gamma \quad \text{and} \\ &B_m = 4\Gamma.\end{aligned} \tag{7}$$

Because $\mathrm{CRLB}_{\widehat{\Gamma}}$ varies with the true Γ, which we only know to be in a given range ($\Gamma_{\min}$ to $\Gamma_{\max}$), we desire to select Δ_B and B_m such that the standard deviation of $\widehat{\Gamma}$ across the range is minimized. Fig. 3 shows that, for fixed values of d and σ, estimator

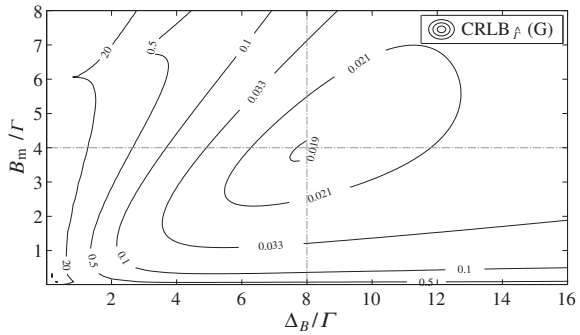

Fig. 2. Theoretical CRLB results. $\mathrm{CRLB}_{\widehat{\Gamma}}$ vs. Δ_B/Γ and B_m/Γ, revealing the location of the minimum. The overall shape of the plot does not vary with Γ; that is, the minimum stays in the same location. Also, the location of the minimum does not vary with d and σ. Parameters used to create the plot are as follows: $\Gamma = 1$ G, $d = 10$, $M = 1024$, $\sigma = 1$.

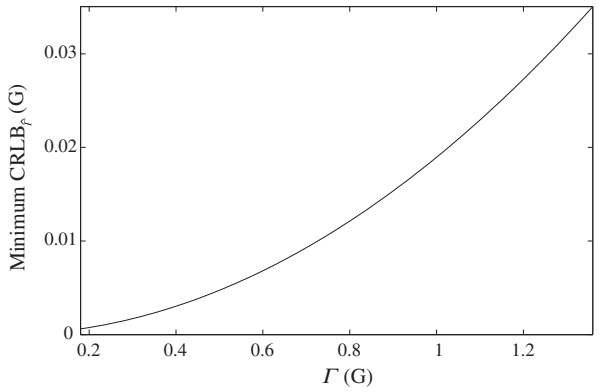

Fig. 3. Best CRLB$_{\hat{\Gamma}}$ possible as a function of Γ, showing Γ from 0.18 G to 1.36 G, which corresponds to the range 0–160 mmHg when using a LiNc-BuO probe [15]. Note that the scale on the vertical axis is determined by d and σ; values are shown here for $d = 10$ and $\sigma = 1$.

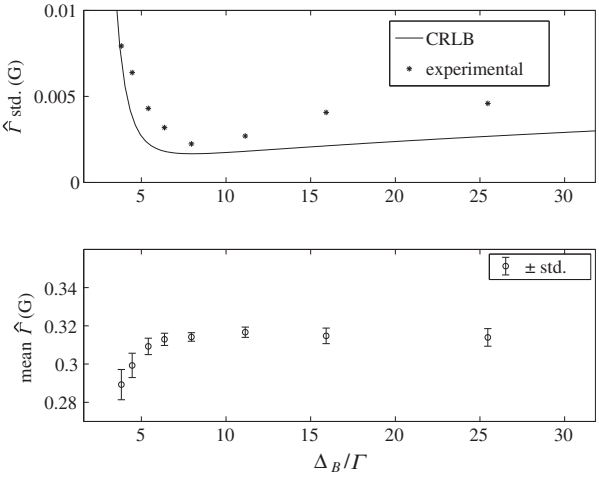

Fig. 4. Comparison of experimental and theoretical results, with $B_m \approx 1.24\ \text{G} \approx 4\Gamma$. Top panel: standard deviation results; bottom panel: experimental results only, means and standard deviations.

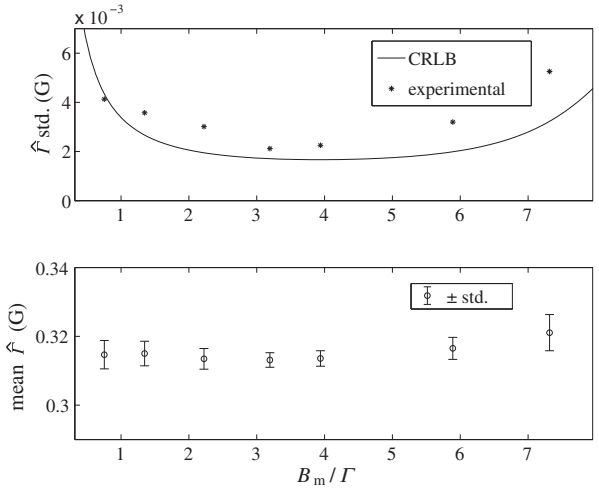

Fig. 5. Comparison of experimental and theoretical results, with $\Delta_B = 2.5\ \text{G} \approx 8\Gamma$. Top panel: standard deviation results; bottom panel: experimental results only, means and standard deviations.

performance is better at lower values of Γ, and suggests that optimizing the parameters for Γ_{max} will minimize the worst-case estimation error across $[\Gamma_{min}, \Gamma_{max}]$.

3.2. L-band spectroscopy

The intrinsic linewidth in our experiment was $\Gamma = 0.315$ G. A variety of scans were taken with $\Delta_B = 2.5\ \text{G} \approx 8\Gamma$ while varying B_m; likewise, a variety of scans were taken with $B_m \approx 1.24\ \text{G} \approx 4\Gamma$ while varying Δ_B. As mentioned earlier, both the scan time ($T = 3.9$ s) and the number of samples per scan ($M = 1024$) were kept fixed. Twelve scans were performed at each combination of Δ_B and B_m.

Joint estimates of d,Γ, and B_m were calculated by curve fitting using Eq. (6). As expected, the estimated values $\widehat{B}_m$ were different from the nominal B_m values set by the user but the difference was within 3%. Figs. 4 and 5 show the results, along with comparison to the theoretical bound. The experimental results are consistent with the theory. For illustration, Fig. 6 compares standard deviation in the estimation of Γ for three selected combinations of B_m and Δ_B.

4. Discussion

Previous discussions of modulation amplitude have focused on increasing traditional figures of merit such as SNR and peak-to-peak signal strength [16]. Fig. 7 illustrates how using these

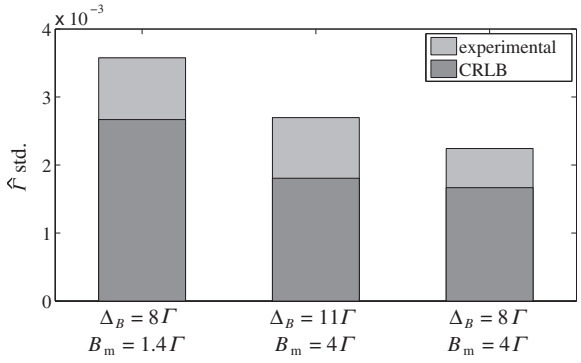

Fig. 6. Standard deviation of $\widehat{\Gamma}$ for three different combinations of B_m and Δ_B. As predicted by theory, $B_m = 4\Gamma$ and $\Delta_B = 8\Gamma$ provide the lowest standard deviation of $\widehat{\Gamma}$. The relative difference in the scaling of experimental and CRLB values is due to the different values of d and σ associated with experimental and theoretical results.

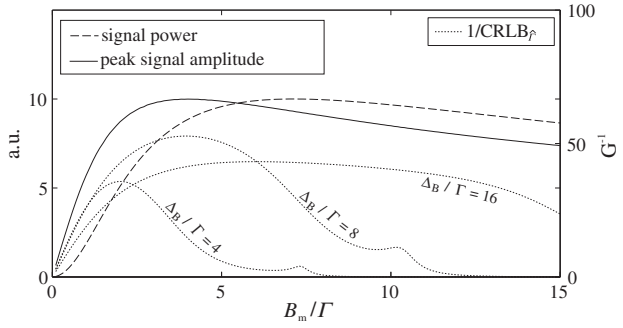

Fig. 7. Comparison of several figures of merit as functions of B_m/Γ. The vertical scale on the left belongs to independently normalized signal power and peak signal amplitude, while the vertical scale on the right belongs to CRLB$_{\hat{\Gamma}}$. To compute CRLB$_{\hat{\Gamma}}$, we selected $\sigma = 1$, $d = 10$, $M = 1024$, and $\Gamma = 1$ G. Note that maximizing peak signal amplitude is a suitable surrogate metric for estimation performance only when sweep width is optimized, i.e., $\Delta_B = 8\ \Gamma$.

figures of merit may not lead to optimal estimator performance. Selecting B_m to maximize signal power (sum-of-squares) does not lead to optimal performance, and selecting B_m to maximize peak signal strength may lead to optimal performance, but only if used in conjunction with the correct value of Δ_B, i.e., $\Delta_B = 8\Gamma$.

The presented CRLB sensitivity analysis determines values of B_m and Δ_B that generate optimal results in terms of standard deviation of the estimated linewidth, which is achieved by selecting a combination of B_m and Δ_B that minimizes $\mathrm{CRLB}_{\widehat{\Gamma}}$. The results (Eq. (7)) were computed with $M = 1024$; the optimal parameters do not vary with M as long as the step-size of the field sweep is considerably smaller than Δ_B. Also, the optimal parameter values of B_m and Δ_B are independent of both signal amplitude d and noise standard deviation σ, which are positive scalar multipliers of $\mathrm{CRLB}_{\widehat{\Gamma}}$ that affect the scaling but not the location of the minimum (Fig. 2). Because the scan time T does not alter the lineshape f but only changes the normalized noise standard deviation, i.e., $\frac{\sigma}{d} \propto \frac{1}{\sqrt{T}}$, the optimal parameter values are also independent of the scan time, provided that the sweep rate does not fall into the rapid-scan regime.

Although we have used $\mathrm{CRLB}_{\widehat{\Gamma}}$ as a figure of merit, equivalent acquisition times can also be computed for comparing various selections of B_m and Δ_B. For $B_m = 4\Gamma$, $\Delta_B = 16\Gamma$, for example, the value of $1/\mathrm{CRLB}_{\widehat{\Gamma}}$ is 78.4% of the $1/\mathrm{CRLB}_{\widehat{\Gamma}}$ value associated with $B_m = 4\Gamma$, $\Delta_B = 8\Gamma$ (Fig. 7). Since $\mathrm{CRLB}_{\widehat{\Gamma}} \propto \frac{\sigma}{d}$ and $\frac{\sigma}{d} \propto \frac{1}{\sqrt{T}}$, a 16Γ scan would require 62.4% longer acquisition time as compared to an 8Γ scan for equivalent accuracy in estimated linewidth. For reference, Fig. 8 shows an experimental EPR spectrum, modulated with the optimal B_m, with the optimal sweep window denoted.

As noted in Section 2.1, the actual value of B_m, in general, is not precisely known and varies slightly but unpredictably from the nominal value set the user. Therefore, setting the $B_m = 4\Gamma$ might not be possible, but the smooth nature of $\mathrm{CRLB}_{\widehat{\Gamma}}$ vs. B_m curve ensures that a $B_m \approx 4\Gamma$ value would only result in a marginal drop in the performance. For applications in which B_m might be precisely controlled, the resulting optimal values of B_m and Δ_B are significantly different from the ones mentioned above. Specifically, sweep width and field modulation amplitude should be set to 4.7Γ and 1.6Γ, respectively, when the value of B_m is precisely known and need not be estimated. The CRLB analysis for known B_m is similar to the one presented here and is omitted for brevity. The results for both the cases, i.e., known and unknown B_m, are summarized in Table 1.

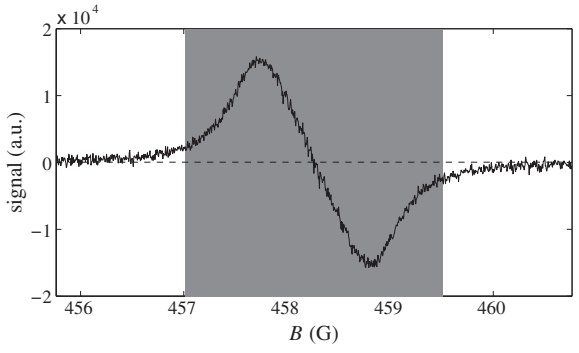

Fig. 8. An EPR spectrum collected on a CW L-band spectrometer with $\Gamma \approx 0.315$ G, optimally modulated with $B_m \approx 1.24\,\mathrm{G} \approx 4\Gamma$. The highlight denotes the optimal sweep width $\Delta_B = 2.5\,\mathrm{G} \approx 8\Gamma$.

Table 1
Optimal parameters depending on whether B_m is estimated or known in advance.

	Estimating d, Γ, and B_m	Estimating d and Γ; B_m is known
Δ_B	8Γ	4.73Γ
B_m	4Γ	1.57Γ

Although the reported results are valid only for the listed set of assumptions, a similar analysis can be performed for a different set of assumptions. For example, effects of modulation frequency, when not negligible, can be included by modifying f (Eq. (1)) accordingly. Likewise, a similar analysis can be conducted when multiple modulation harmonics are simultaneously considered [17].

5. Conclusions

Experimental settings for field modulation amplitude, B_m, and sweep width, Δ_B, should be set jointly for the best performance in CW EPR. We have used standard deviation of linewidth estimation error, as predicted by the Cramér-Rao lower bound, to select B_m and Δ_B. For cases where B_m cannot be controlled precisely, the optimal parameters for a modulation-distorted first-harmonic Lorentzian are found to be $\Delta_B = 8\Gamma$ and $B_m = 4\Gamma$, with Γ being the HWHM linewidth. We have also shown that, given Γ in a range from Γ_{min} to Γ_{max}, the standard deviation of the worst-case estimation of linewidth is minimized by designing for Γ_{max}: $\Delta_B = 8\Gamma_{max}$ and $B_m = 4\Gamma_{max}$. Further, for cases where B_m is precisely known, the preferred experimental settings result in a much narrower sweep width: $\Delta_B = 4.7\Gamma$ and $B_m = 1.6\Gamma$.

Acknowledgments

We thank Dr. Periannan Kuppusamy for use of laboratory equipment at the Davis Heart and Lung Research Institute. This work was supported by NIH Grant EB008836.

References

[1] S. Eaton, G. Eaton, L. Berliner (Eds.), Biomedical EPR, Part A: Free Radicals, Metals, Medicine and Physiology, Kluwer Academic, New York, 2004.
[2] H. Swartz, Measurement of Oxygen In vivo using EPR Techniques *in* In Vivo EPR (ESR): Theory and Applications, Kluwer Academic, New York, 2003. Chap. 15, pp. 404–440.
[3] M. Elas, R. Bell, D. Hleihel, E. Barth, C. McFaul, C.H.J. Bielanska, K. Pustelny, K. Ahn, C. Pelizzari, M. Kocherginsky, H. Halpern, Electron paramagnetic resonance oxygen image hypoxic fraction plus radiation dose strongly correlates with tumor cure in FSa fibrosarcomas, Int. J. Radiat. Oncol., Biol., Phys. 71 (2008) 542–549.
[4] R. Ahmad, P. Kuppusamy, Theory, instrumentation, and applications of electron paramagnetic resonance oximetry, Chem. Rev. (2010) 3212–3236.
[5] S. Subramanian, M. Krishna, Dancing with the electrons: time-domain and CW in vivo EPR imaging, Magn. Reson. Insights 2 (2008) 43–74.
[6] C.P. Poole Jr., Electron Spin Resonance: A Comprehensive Treatise on Experimental Techniques, Dover, Mineola, 1997. Chap. 7, pp. 259–288.
[7] H. Wahlquist, Modulation broadening of unsaturated Lorentzian lines, J. Chem. Phys. 35 (1961) 1708–1710.
[8] B. Robinson, C. Mailer, A. Reese, Linewidth analysis of spin labels in liquids: I. Theory and data analysis, J. Magn. Reson. 138 (1999) 199–209.
[9] C. Mailer, B. Robinson, B. Williams, H. Halpern, Spectral fitting: the extraction of crucial information from a spectrum and a spectral image, Magn. Reson. Med. 49 (2003) 1175–1180.
[10] J. Joshi, J. Ballard, G. Rinard, R. Quine, S. Eaton, G. Eaton, Rapid-scan EPR with triangular scans and Fourier deconvolution to recover the slow-scan spectrum, J. Magn. Reson. 175 (2005) 44–51.
[11] S. Som, L. Potter, R. Ahmad, P. Kuppusamy, A parametric approach to spectral-spatial EPR imaging, J. Magn. Reson. 186 (2007) 1–10.
[12] P. Stoica, R. Moses, Spectral Analysis of Signals, Prentice Hall, Upper Saddle River, 2005.
[13] R. Pandian, N. Parinandi, G. Ilangovan, J. Zweier, P. Kuppusamy, Novel particulate spin probe for targeted determination of oxygen in cells and tissues, Free Radical Biol. Med. 35 (2003) 1138–1148.
[14] J. Freed, D. Leniart, J. Hyde, Theory of saturation and double resonance effects in ESR spectra. III. RF coherence and line shapes, J. Chem. Phys. 47 (1967) 2762–2773.
[15] R. Pandian, V. Dang, P. Manoharan, J. Zweier, P. Kuppusamy, Effect of nitrogen dioxide on the EPR property of lithium octa-n-butoxy 2,3-naphthalocyanine (LiNc-BuO) microcrystals, J. Magn. Reson. 181 (2006) 154–161.
[16] R. Nielsen, B. Robinson, The effect of field modulation on a simple resonance line shape, Concepts Magn. Reson. Part A 23A (2004) 38–48.
[17] R. Ahmad, S. Som, E. Kesselring, P. Kuppusamy, J. Zweier, L. Potter, Digital detection and processing of multiple quadrature harmonics for EPR spectroscopy, J. Magn. Reson. 207 (2010) 322–331.